PCCP

Accepted Manuscript

This article can be cited before page numbers have been issued, to do this please use: X. Hu, J. Zuo, C. Xie, R. Dawes, H. Guo and D. Xie, *Phys. Chem. Chem. Phys.*, 2019, DOI: 10.1039/C9CP02206F.

ROYAL SOCIETY OF CHEMISTRY

rsc.li/pccp

DOI: 10.1039/C9CP02206F

Submitted to *Phys. Chem. Chem. Phys.* 4/18/2019, revised on 6/10/2019

An *ab initio* based full-dimensional potential energy surface for OH + O_2 ⇄ HO_3 and low-lying vibrational levels of HO_3

Xixi Hu,[1,2,*] Junxiang Zuo,[1] Changjian Xie,[2] Richard Dawes,[3,*] Hua Guo,[2] and Daiqian Xie[1]

[1] *Institute of Theoretical and Computational Chemistry, Key Laboratory of Mesoscopic Chemistry, School of Chemistry and Chemical Engineering, Nanjing University, Nanjing 210093, China*

[2] *Department of Chemistry and Chemical Biology, University of New Mexico, Albuquerque, New Mexico 87131, USA*

[3] *Department of Chemistry, Missouri University of Science and Technology, Rolla, Missouri 65409, USA*

Corresponding authors: xxhu@nju.edu.cn, dawesr@mst.edu

View Article Online
DOI: 10.1039/C9CP02206F

Abstract

To provide an in-depth understanding of the HO_3 radical and its dissociation to $OH + O_2$, a six-dimensional potential energy surface has been constructed by fitting 2087 energy points for the electronic ground state of HO_3 (X^2A'') using the permutation invariant polynomial-neural network (PIP-NN) approach. The energy points were calculated using an explicitly-correlated and Davidson-corrected multi-reference configuration interaction method with the correlation-consistent polarized valence double zeta basis (MRCI(Q)-F12/VDZ-F12). On the PES, the *trans*-HO_3 isomer is found to be the global minimum, 33.0 cm^{-1} below the *cis*-HO_3 conformer, which is consistent with previous high-level theoretical investigations. The dissociation to the $OH + O_2$ asymptote from both conformers is shown to be barrierless. As a benchmark from a recently developed high-accuracy thermochemistry protocol, D_0 for *trans*-HO_3 is calculated to be 2.29±0.36 kcal mol^{-1}, only slightly deeper than the value of 2.08 kcal mol^{-1} obtained using the PES, and in reasonable agreement with the experimentally estimated value of 2.93±0.07 kcal mol^{-1}. Using this potential energy surface, low-lying vibrational energy levels of HO_3 are determined using an exact quantum Hamiltonian and compared with available experimental results.

View Article Online
DOI: 10.1039/C9CP02206F

I. INTRODUCTION

The hydrotrioxyl radical (HOOO or HO_3) has been implicated in many different gaseous environments such as combustion[1] and Earth's atmosphere.[2] It can be formed as an adduct of the OH and O_2 radicals, potentially serving as a reservoir of the OH radical in the atmosphere.[3] The effective concentration of OH is a crucial parameter in atmospheric models. However, the HO_3 radical species is very weakly bound, and its detection in the gas phase was first reported in 2002.[4] Since then, there have been several experimental investigations on this elusive radical species in the isolated form using various spectroscopic techniques.[5-15] Rotational transitions of *trans*-HO_3 and *trans*-DO_3 were observed by Endo and coworkers using Fourier-transform microwave spectroscopy, which allowed an estimation of its geometric parameters with some constraints.[5] Their experiments were extended more recently by McCarthy and coworkers who included additional isotopologues in the analysis to obtain a better determined structure.[11, 15] Interestingly, spectral features of the *cis*-conformer were found experimentally in neither gas phase experiments,[5, 11] nor in He droplets.[12] Lester and coworkers reported observations of fundamental, overtone, and combination vibrational transitions of HO_3 and DO_3 using a double resonance technique.[8, 9] In these experiments, transitions assigned to both the *trans* and *cis* conformers were reported.

The kinetics of the OH and O_2 association to form HO_3 has also been examined in detail.[16, 17] These experiments found a negative temperature dependence of the association rate constant, suggesting a barrierless reaction path. In addition, the dissociation energy of HO_3 (D_0) was estimated from the equilibrium constant to be 2.93±0.07 kcal mol^{-1}. This

View Article Online
DOI: 10.1039/C9CP02206F

value is significantly lower than previously reported upper bounds from infrared action spectroscopy (5.31 to 6.12 kcal mol^{-1}).[6, 7, 9]

The HO_3 system has proven to be a very challenging system for *ab initio* characterization.[18] For example, the central O-O equilibrium distance r_e depends sensitively on the level of theory,[5, 19-22] presumably due to its largely non-covalent nature. Furthermore, due to the weakness of the bond, a significant difference can be anticipated between the equilibrium distance r_e and the ground state vibrationally averaged value r_0. Indeed, the equilibrium geometry of *trans*-HO_3 obtained at the state-of-the-art coupled cluster singles, doubles and perturbative triples level in the complete basis set limit (CCSD(T)/CBS)[20] poorly matches the most recent spectroscopically derived structure.[11] In addition, previously calculated D_e values range from 4 to 10 kcal mol^{-1},[21, 23-26] although the most recent multi-reference calculations[22, 27, 28] have started to converge toward values consistent with the experimental D_0 result.[16] Several *ab initio* studies,[29-31] including the most recent equation-of-motion CCSD (EOM-CCSD) calculations,[25] predicted a significant energy barrier for the adiabatic dissociation of HO_3 to OH + O_2 on the ground electronic state PES. The existence of such a barrier is inconsistent with the observed negative temperature dependence of the HO_3 formation rate coefficient.[16, 17] More recently, Anglada *et al*. found no such barrier at the complete active space 2nd order perturbation theory (CASPT2) level of theory.[26] Another issue is the relative stability between the *trans*- and *cis*-HO_3 isomers. In 2011, Varandas explored the minimum energy path for HO_3 isomerization using high-level *ab initio* methods extrapolated to the complete basis set limit.[32] For single-reference methods, the *cis*-HO_3 conformer was found to be slightly

View Article Online
DOI: 10.1039/C9CP02206F

more stable than its *trans* conformer,[32] with one exception.[33] However, multi-reference calculations predicted that *trans*-HO_3 is more stable than the *cis* counterpart, in agreement with the available experimental evidence.[10] These results suggested a large multi-reference character in this system.

Despite the large number of theoretical studies of the HO_3 radical reported so far, to our knowledge, none simultaneously reproduces all of the available experimental data with sufficient accuracy. Furthermore, a quantitative theory-experiment comparison is not possible, especially for this floppy system,[13, 15] without a quantum mechanical treatment of the nuclear dynamics, which requires a full-dimensional global potential energy surface (PES). To this end, various attempts have been made.[13, 24, 31, 34] In 2001, Yu and Varandas constructed a global PES for the electronic ground state of HO_3 using the quadratic configuration interaction with singles, doubles, and perturbative triples (QCISD(T)/CBS) method.[31] Two stable planar HO_3 isomers were found on that PES, but *cis*-HO_3 is more stable than the *trans* one. In addition, it predicted a dissociation barrier, which is inconsistent with the later experimental evidence. Another analytical PES in the many-body expansion form was developed by fitting about 28000 density functional theory points with the HCTH functional and aug-cc-pVTZ basis set.[24] However, the predicted D_0 of 6.15 kcal mol^{-1} is too large and the central O-O bond length of 1.610 Å for *trans*-HO_3 is too short.

In this publication, we describe benchmark explicitly-correlated and Davidson-corrected multi-reference configuration interaction (MRCI(Q)-F12/CBS) calculations that are entirely consistent with all experimental observations (central O-O distance,

View Article Online
DOI: 10.1039/C9CP02206F

barrierless association path, and well depth). Furthermore, we apply a recently developed high-accuracy thermochemistry protocol to the *cis* and *trans* isomers to help benchmark their absolute and relative stabilities and gain insight into their electronic structure. We also report a new PES that includes key stationary points of the HO_3 system and the OH + O_2 dissociation channel based on thousands of *ab initio* points obtained at the MRCI(Q)-F12/VDZ-F12 level of theory. The method employed for the PES uses a smaller basis set than the benchmark calculations due to the high cost of the latter, but is still reasonably accurate and accounts for the significant multi-reference character of this system. Using this new PES, exact quantum dynamics calculations (J=0) are performed to determine the low-lying vibrational levels for both HO_3 and DO_3. The overall agreement with the available experimental data is quite satisfactory. This work is organized as follows. In Section II, we describe the details of the electronic structure calculations and fitting approach, as well as the quantum dynamical methods for determining the vibrational levels. Section III presents and discusses the calculated results. A short conclusion is given in the final section.

II. COMPUTATIONAL DETAILS

A. *Ab initio* calculations

As discussed above, it is quite challenging to choose a good electronic structure method to construct an accurate global PES for HO_3, since affordable *ab initio* approaches used in the literature fall short in one respect or another. For example, single-reference methods (QCISD, QCISD(T), and CCSD(T)) predicted too short a length for the central O-O bond, regardless of the basis size.[19, 20] The association of OH and O_2 was predicted

View Article Online
DOI: 10.1039/C9CP02206F

to have a significant (spurious) barrier at the level of EOM-CCSD.[25] On the other hand, dynamic correlation due to high-order excitations was found to be essential.[26] Given the previously reported issues with single reference methods such as the geometries of minima and spurious barriers, for the global PES we seek an affordable, robustly convergent, and reasonably accurate method that accounts for the multi-reference character of the system. In addition, to better understand the performance of various methods as well as the sources of discrepancies and the relative contributions of different energy components, we performed some benchmark calculations on the *cis* and *trans* isomers using a recently developed high-accuracy thermochemistry protocol.[35]

The explicitly correlated MRCI-F12 method[36] was selected to carry out electronic structure calculations using the VDZ-F12, VTZ-F12, and VQZ-F12 basis sets.[37] The F12 version of MRCI is known to converge quickly with respect to basis size,[38] which is important for our calculations because of the large number of electrons and active space orbitals. The basis set used here for the full PES is not particularly large, but tests presented below indicate it is sufficient to provide a reasonably accurate description without overwhelming computational costs. Davidson corrections (Q) using rotated reference energies were included.[39]

The doublet electronic ground state of HO_3 is of A″ symmetry in the C_s group, which becomes degenerate with the ^{2}A′ state for the separated OH and O_2 fragments. Adiabatic dissociation in the C_s group follows: $HO_3(^2A'') \rightarrow O_2\left(^3\Sigma_g^-\right) + OH(^2\Pi)$. Diabatically, the ground state of HO_3 correlates to an excited state of the molecular oxygen product: $HO_3(^2A'') \rightarrow O_2\left(^1\Delta_g\right) + OH(^2\Pi)$, resulting in an avoided crossing in the

View Article Online
DOI: 10.1039/C9CP02206F

transition region among the A″ states, analogous to that seen in ozone.[40, 41] The low-lying states of the OH and O_2 fragments include the ground $^2\Pi$ state of OH and the ground $^3\Sigma_g^-$, and excited $^1\Delta_g$ and $^1\Sigma_g^+$ states of O_2. Altogether, these combine to form eight doublet states ($4\ ^2A' + 4\ ^2A''$) with an asymptotic degeneracy pattern of 2 ($^2A' + ^2A''$), 4 ($2\ ^2A' + 2\ ^2A''$), 2 ($^2A' + ^2A''$).

Thus, in order to smoothly represent the switching state character, for the ground state of $HO_3(^2A'')$, an eight-state ($4^2A' + 4^2A''$) dynamically weighted state-averaged completed active space self-consistent field (DW-SA-CASSCF) reference[42, 43] was used with the 2s orbitals of O atoms closed, but correlated in the MRCI. This level of theory is still quite demanding computationally, even with a double zeta basis, a single-point energy takes about six hours of CPU time with 12 cores (Intel Xeon E5-2680 v3 @ 2.50 GHz).

In order to build a globally accurate PES with reasonable computational costs, especially for such a high-dimensional system, it is vital to sample the *ab initio* points prudently. To this end, a much less expensive quantum chemistry method employing the M06-L functional[44] and the cc-pVTZ basis set (about 1 minute per point on a 12 core node) was first used to generate a low-level PES, using the same fitting method discussed below. In general, the M06-L results agree only qualitatively with the high-level theoretical results. The comparisons of geometries and harmonic frequencies are listed in Tables S-I and S-II, respectively, in Supporting Information (SI). As shown in these tables, the M06-L PES significantly overestimate the energy of the cis isomer and the isomerization barrier. Tests however confirmed that the M06-L method was sufficiently accurate to serve as a guide. The geometries for the MRCI+Q calculations were then

View Article Online
DOI: 10.1039/C9CP02206F

selected using an energy criterion to sample the relevant region for the $HO_3 \rightarrow OH + O_2$ reaction. In this work, both the MOLPRO[45] and the Gaussian[46] suites of electronic structure programs were used.

B. Fitting of the potential energy surface

To provide an analytical representation of these *ab initio* points, analytic PESs were constructed using the permutation invariant polynomial-neural network (PIP-NN) method.[47-49] The PIP-NN approach enforces permutation symmetry among the three oxygens in the NN fitting by employing a special set of symmetry functions as the input vector, rather than the internuclear distances themselves. The symmetry functions are PIPs of Morse variables[50] defined as $y_i = \exp(-r_i/\alpha)$, where r_i is an internuclear distance between two nuclei with a chosen α of 2.5 bohr. For this system, 22 PIPs (up to the third order) were used for this AB_3 system.

In the NN fitting, the data were divided randomly into three sets, namely the training (90%), validation (5%), and testing (5%) sets. Different NN architectures with two hidden layers were tested. For each architecture, 100 different training calculations were performed with the ‘‘early stopping’’ method.[51] Furthermore, batches of trajectories at various energies were dispatched to search for unphysical regions of the PES resulting from a lack of *ab initio* data points. New configurations generated by the trajectories were selected or discarded according to both energy and geometry criteria. To impose the energy criterion, the root-mean-square error (RMSE) among the three saved fits at the new point was evaluated and if it was larger than a predetermined value, *e.g.*, 2 kcal mol^{-1}, this configuration was selected, as it indicates a large uncertainty at this point

View Article Online
DOI: 10.1039/C9CP02206F

presumably due to the lack of points. The geometry criterion was enforced by the Euclidean distance defined in terms of the internuclear distances between a point $\vec{r}_i$ and those $\vec{r}'_i$ in the existing data sets. If this value is smaller than 0.05 Å, this point is discarded because it is too close to an existing point already in the data set. A weighting function of the form $w_i = \left[1.2/\left(E_i + 0.9\right)\right]^2$ (energy unit is eV) was employed to ensure that points in low-energy regions have large weights during the training. This procedure was iterated until the results converged. Finally, 2087 points were collected in this manner and fit with the NN structure of 20 and 20 neurons in the first and second hidden layers.

C. Vibrational Hamiltonian and diagonalization

The vibrational energy levels of HO_3 on this new PES were determined using iterative methods.[52] Briefly, calculations were performed with an exact full-dimensional quantum Hamiltonian (J=0) in the body-fixed (BF) frame. For HO_3, diatom-diatom Jacobi coordinates were used, as shown in Fig. 1(b), in which r_1 and r_2 are the diatomic bond lengths, r_3 is the distance between the center of masses of the two diatoms, θ_1 and θ_2 are the polar bending angles, and φ is the out-of-plane torsional angle. This coordinate system is ideally suited for studying the dissociation/association dynamics. The $J = 0$ Hamiltonian for a diatom-diatom system in these Jacobi coordinates is given by ($\hbar$=1)

$$\hat{H} = \sum_{i=1}^{3} -\frac{1}{2\mu_i}\frac{\partial^2}{\partial r_i^2} + \sum_{i=1}^{3}\frac{\hat{j}_i^2}{2\mu_i r_i^2} + V(r_1, r_2, r_3, \theta_1, \theta_2, \varphi), \quad (1)$$

where μ_1, μ_2, and μ_3 are the corresponding reduced masses. $\hat{j}_1$ and $\hat{j}_2$ are the angular momentum operators for r_1 and r_2, respectively, and $\hat{j}_3^2 = \left(\hat{j}_1 + \hat{j}_2\right)^2$. V is the potential energy defined in the Jacobi coordinates. To ensure an efficient propagation, the Hamiltonian was discretized in terms of a potential optimized discretized variable

View Article Online
DOI: 10.1039/C9CP02206F

representation (PODVR) for the three radical coordinates and uncoupled spherical harmonics for the angular coordinates.[53]

The eigen-problem was solved using either the Lanczos algorithm[54] or the real Chebyshev propagation.[55] Since these methods have been extensively discussed in the literature,[52] no further details are given here. It suffices to note that the eigenvalues are first calculated and the eigenfunctions are, when needed, then obtained in subsequent propagations. The basis size used in these calculations, which was tested for convergence, consists of 6 PODVRs in r_1, 4 PODVRs in r_2, 30 PODVRs in r_3, $j_{1,\max} = 45$ in θ_1, $j_{2,\max} = 20$ in θ_2, and $|m|_{\max} = 20$ in φ. The j_i and m are the usual quantum indices in associated Legendre polynomials. We emphasize that the parity of the system is taken into consideration in the calculations, as described in our earlier work.[56]

III. RESULTS AND DISCUSSION

A. *Ab initio* calculations

Geometries along the dissociation path were numerically optimized in internal coordinates (see Figure 1) at the MRCI-F12 level with the relaxed reference Davidson correction and the VTZ-F12 basis set. Additional tests were performed at each optimized geometry using the V*n*Z-F12 (n=2-4) basis series. The dissociation process for $HO_3 \rightarrow OH + O_2$ was found to be barrierless, consistent with the kinetics data.[16, 17] The well depth (D_e) of the *trans*-HO_3 with the VTZ-F12 basis is 4.41 kcal mol^{-1}. The CBS energy for each relaxed structure along the path was estimated by calculating single-point MRCI-F12/VQZ-F12 energies (D_e = 4.63 kcal mol^{-1}) and using the l^{-3} extrapolation formula. Thus, the CBS(VTZ/VQZ) well depth of the *trans*-HO_3 is 4.79 kcal mol^{-1}. The *trans-cis*

View Article Online
DOI: 10.1039/C9CP02206F

differences at the CBS level (-0.077 kcal mol^{-1}) was also determined.

Although it was determined that a multireference method is preferred to construct the global PES, it is also of interest to better characterize the single reference electronic structure of the *cis* and *trans* isomers. Thus, a slight modification of a recently developed thermochemistry protocol was applied.[35] The protocol employs explicitly-correlated coupled-cluster theory with up to five zeta basis sets and includes contributions from: core-electron correlation, high-order correlation (up to CCSDT(Q)), scalar relativistic and spin-orbit effects, non-Born-Oppenheimer effects (through a diagonal Born-Oppenheimer correction), and vibrational zero-point energy (VZPE). Here as a slight modification we estimate VZPE via VPT2 at the UCCSD(T)-F12b/VDZ-F12 level. The protocol has been benchmarked for 200 small gas-phased molecules using the Active Thermochemical Tables[57] and assigned a 95% confidence interval of ±0.36 kcal mol^{-1} in applicable systems. The *cis* and *trans* isomers of HO_3 were found to lie on the very edge of applicability of the single-reference based scheme which employs the criteria of Jiang *et al*.[58] The protocol assigns excessive multireference character to cases with coupled-cluster diagnostics $T_1 >$ 0.05, $D_1 > 0.15$, and a contribution of high-order correlation (beyond CCSD) to total atomization (%TAE), of more than 10%. In our results, for *trans*-HO_3, T_1=0.043, D_1=0.150, and %TAE=9.3%. For *cis*-HO_3, values of T_1=0.043, D_1=0.159, and %TAE=8.5% were obtained. The calculated 0 K enthalpies of formation for *trans* and *cis*-HO_3 are 27.642 and 28.343 kJ/mol respectively. Relative to O_2 + OH, this corresponds to well-depths of 2.294±0.36 and 2.127±0.36 kcal mol^{-1} with the more stable *trans* isomer found 59 cm^{-1} below *cis*. These results are in contrast to more limited single-reference

View Article Online
DOI: 10.1039/C9CP02206F

calculations mentioned above that predicted the *cis* isomer to be more stable. Given that the diagnostics for multireference character are close to their limits, one might assume that in this case swapping in multireference energy components would improve the accuracy of the protocol. Note however, that in our employed MRCI-F12 calculations, the inclusion of the Davidson correction contributes a significant fraction of the well depth (roughly 30%). Thus we conclude that the HO_3 system not only has a complicated multiconfigurational electronic structure, but that even with a multireference description, high-order correlation from excitations beyond doubles is important. Unfortunately, at this time there are no affordable, rigorous approaches to capture high-order correlation in multireference CI.

As mentioned above, diabatically the ground electronic state connects to an excited state of the molecular oxygen product: $HO_3(^2A'') \rightarrow O_2\left(^1\Delta_g\right) + OH(^2\Pi)$, somewhat analogous to the dissociation of ozone for which an avoided crossing with a high-lying state has been implicated as the cause of a spurious reef feature in some PESs.[40, 41] To explore this further in HO_3, the three lowest $^2A''$ states were computed along the dissociation path at the MRCI(Q)-F12/VTZ-F12 level (see Figure 2). Analysis of the orbitals and CI vector confirmed the switch in character between the ground and first excited states of the same symmetry along this path. Interestingly, the corresponding nonadiabatic coupling matrix element (NACME) between the two states (plotted in Figure 3) peaks at a bond distance of around 2 Å with a shape reminiscent of the spurious barrier seen in EOM-CC calculations.[25]

Unfortunately, the costs of calculations with basis sets larger than VDZ-F12 are

View Article Online
DOI: 10.1039/C9CP02206F

prohibitive at this time, considering the thousands of points required to describe the PES. However, energies computed with the VDZ-F12 basis were further from the CBS benchmarks than was deemed acceptable for a spectroscopic study. For example, the *trans* well depth (D_e) which follows the progression 4.41, 4.63, and 4.79 kcal mol^{-1} for VTZ-F12, VQZ-F12 and CBS respectively is only 3.90 kcal mol^{-1} at the VDZ-F12 level. Thus, to improve the accuracy of the PES, using the benchmark data and studying the basis dependence of the various energy components, an effective scaling procedure was determined, constrained due to costs to include only contributions from the VDZ-F12 calculations.

To give a balanced description of the well shapes and depths, as well as the isomerization path from the *trans* to *cis* geometries that is as close as possible to the CBS benchmarks, we scaled the correlation energy (roughly defined as the difference between the CASSCF reference and the MRCI(Q_{rot})-F12 value) by a factor of 1.059. This scaling yields a value for *trans* D_e of 4.79 kcal mol^{-1} which is the same as the CBS value. The results so obtained are in general accord with the measurement of Le Picard *et al.* (D_0=2.93±0.07 kcal mol^{-1}).[16] This scaling scheme was then used to generate the global PES.

B. Properties of PES

Multiple fittings were performed and the RMSE fitting error for the final averaged PES from the three best PIP-NN fits is 7.4 meV (59.7 cm^{-1}). The fitting errors of all points are shown in Figure 4.

The resulting ground state PES of HO_3 has two planar conformers, namely *trans*-

View Article Online
DOI: 10.1039/C9CP02206F

HO_3 and *cis*-HO_3. The optimized isomerization path is displayed in Figure 5 as a function of the torsion angle, with all other internal coordinate optimized. Here, φ_{OOOH}=0° corresponds to the *cis*-geometry while 180° refers to the *trans* conformer. Both the *ab initio* data and fitted PES predict that *trans*-HO_3 is more stable than the *cis* conformer, in agreement with the available experimental evidence.[10] The *cis*-HO_3 conformer, lying 32.98 cm^{-1} above the *trans*-HO_3 one, is connected *via* a saddle point (i-TS) located at the φ_{OOOH}=81.4° with a barrier of 365.22 cm^{-1}, consistent with the CBS values obtained by us and reported previously by Varandas.[32]

The dissociation curves for both *trans*-HO_3 and *cis*-HO_3 are presented in Figure 6. No barrier is observed along either of the *trans*- and *cis*-HO_3 dissociation paths. The dissociation energy D_e of the PES is 1675 cm^{-1} (4.79 kcal mol^{-1}) for *trans*-HO_3, which is very close to the CBS value (4.7897 kcal mol^{-1}) and slightly larger than that for *cis* (4.7127 kcal mol^{-1}).

The stationary point geometries (*trans*-HO_3, *cis*-HO_3, and i-TS) are listed in Table I in internal coordinates, together with previous theoretical and experimental values. The corresponding energies relative to *trans*-HO_3 are also displayed. From the data in Table I, it is clear that the bond lengths and angles calculated by the MRCI(Q)-F12/VDZ-F12 method in this work are in good agreement with the literature values. The long O′–O″ bond length of *trans*-HO_3 (1.6584 Å) well reproduces the commonly accepted experimental value (1.688 Å).[5] The *cis* isomer has a significantly shorter O′-O″ bond length of 1.5726 Å.

The harmonic frequencies at each stationary point are compared with the *ab initio*

View Article Online
DOI: 10.1039/C9CP02206F

results at the MRCI(Q)-F12/VTZ level of theory in Table II for both HO_3 and DO_3. The agreement is quite good, a testament of the fitting fidelity. The non-planar isomerization transition state (i-TS) has a single imaginary frequency (158.2*i* cm^{-1}). It is important to note that the molecule is quite floppy. Contour plots of the PES in various pairs of Jacobi coordinates with other four coordinates fixed at the equilibrium values of *trans*- HO_3 are shown in Figure 7.

C. Vibrational energy levels

Fundamental frequencies for both the *trans* and *cis* forms of HO_3 and DO_3 calculated on the new PES are compared with those obtained from the IR-UV experiments and previous theoretical results in Table III. Extensive testing was performed on the convergence with respect to the size of the basis, and the results reported here are converged to 1 cm^{-1}. The wavefunctions of those states are shown in Figure 8, where the nodal structures of the wavefunctions were used to make the assignments. The assignments are given in terms of six normal mode quantum numbers: ($n_1n_2n_3n_4n_5n_6$). In particular, n_1, n_2 and n_5 denote the quantum numbers for the stretching modes of the OH, terminal OO and central OO bonds, respectively, n_3 and n_4 represent quantum numbers for the H-O-O and O-O-O bending modes, and n_6 for the torsional vibration. Note that each conformer has its own set of normal modes. The coordinates r_1, r_2, r_3, and θ_1 for the *trans* and *cis* geometries are very similar, while the θ_2 and φ are distinguished for the *trans* and *cis*-HO_3. So the vibrational states can be assigned by the parity and analyzing the positions and node numbers of the wavefunctions. For the *trans*-HO_3, the wavefunction is around θ_2=115° and φ=0°, while the wavefunction of *cis*-HO_3 is near the geometry of

View Article Online
DOI: 10.1039/C9CP02206F

θ_2=81° and φ=180°.

The calculated zero-point energies (ZPEs) are 3582.46 and 3693.81 cm^{-1} for *trans*- and *cis*-HO_3, respectively. After including the ZPE corrections, the *trans*-HO_3 species is still more stable than the *cis* one. The bond dissociation energy D_0, estimated from the D_e and the zero point energies of HO_3 and the two monomers (OH and O_2), is 727.3 cm^{-1} (2.08 kcal mol^{-1}), which is smaller than the experimental estimate (2.93±0.07 kcal mol^{-1}).[16] The error is presumably due to higher-order excitations.

Overall, the vibrational energies of the fundamental levels calculated on our PES are close to those computed on a MRCI force field by Suma *et al*.[22] The torsional mode (ν_6) has the lowest frequency for both conformers, underscoring the floppy nature of the radical. Strong anharmonicity in the torsion mode was found due to the low isomerization barrier. For the central OO stretching mode (ν_5), the fundamental frequencies are predicted to be 261.97 cm^{-1} for *trans*-HO_3 and 264.41 cm^{-1} for *cis*-HO_3, which are about 20 cm^{-1} larger than the experimental values (243.7 cm^{-1} and 243.6 cm^{-1}).[9] The low frequency also reflects the extremely weak bonding between OH and O_2, and the reasonable theory-experiment agreement provides evidence in support of the accuracy of the PES. The OOO bending (ν_4) frequency of the *trans*-HO_3 (482.94 cm^{-1}) is in excellent agreement with the experimental results (481.9 cm^{-1}),[9] but fundamental frequency of ν_4 for *cis*-HO_3 (545.4 cm^{-1}) is 59 cm^{-1} larger than the experimental value. A similarly large difference was also found by Suma *et al*. in their MRCI(Q)/AVQZ calculations.[22] In addition, the calculated fundamental frequency of ν_3 (1043.28 cm^{-1}) is also larger than the experimental result (997.9 cm^{-1}). In general, the calculated frequencies reproduce most experimental values

View Article Online
DOI: 10.1039/C9CP02206F

reasonably well. This agreement supports the assignments of the IR-UV experiment and validates the accuracy of our PES.

Some low-lying vibrational energy levels for both HO_3 and DO_3 are listed in Tables S-I and S-II, respectively, in Supporting Information. Because of the strong intermodal coupling and the low-frequency torsional mode, the density of states increases quite rapidly with energy. All the energy levels below 4240 cm^{-1} for HO_3 and 3600 cm^{-1} for DO_3 are included in the tables, but only the assigned energy levels above these energy cutoffs were presented. Not all states are assignable because of the lack of clear nodal structure and some of our assignments are tentative.

It is interesting to note that each vibrational level is associated with a small energy splitting. For instance, a tiny splitting of 0.004 cm^{-1} is observed in the ground vibrational state of *trans*-HO_3. The splitting increases for higher energy levels. This splitting arises from a multi-dimensional dynamical tunneling of oxygen atoms between the two permutationally equivalent wells for the O-O′ moiety, which removes the degeneracy of the two local vibrational states. These two wells are separated by a significant barrier, which makes the mixing of the two local wavefunctions very weak. This is clearly shown in the (000001) state wavefunctions in Figure 8, where amplitudes in both wells are present.

Overall, the global PES provides a reasonable characterization of the vibrational spectrum. However, it is clear that the agreement with the experimental results is not yet quantitative. The major uncertainties are presumably in the *ab initio* calculations, although the fitting of the *ab initio* points also contains errors. A definitive assessment of the

View Article Online
DOI: 10.1039/C9CP02206F

uncertainty is out of the scope of this work, but it is clear that further improvements are needed to achieve spectroscopic accuracy.

IV. CONCLUSIONS

In this work, we report extensive MRCI calculations with various basis sets that explore the dissociation and isomerization of the HO_3 radical species. It is shown from these *ab initio* calculations that the *trans*-HO_3 conformer is the global minimum and the dissociation pathway is barrierless, consistent with the kinetic data. In addition, the dissociation energy is consistent with the experimental estimation. Analysis of nonadiabatic coupling to an excited state provides insight into the origin of a previously reported spurious barrier along the path. Further characterization of the electronic structure and energies of the two isomers was obtained using a recently developed thermochemistry protocol.

A full-dimensional global PES for HO_3, including the HO + O_2 dissociation asymptote, has been constructed by fitting 2087 MRCI(Q)-F12/VDZ-F12 points using the PIP-NN method. The PES provides an analytic representation of both the isomerization and dissociation pathways. This PES paves the way for studying both the isomerization and dissociation dynamics.

Based on this PES, rigorous quantum dynamics calculations have been carried out to compute the vibrational energy levels of HO_3. Assignments have been attempted for some low-lying levels with six normal mode quantum numbers. The calculated fundamental frequencies of HO_3 and DO_3 are in good agreement with the experimental values obtained by Lester and coworkers. Some of the vibrational modes are strongly anharmonic. The

View Article Online
DOI: 10.1039/C9CP02206F

calculated D_0 value on this PES is slightly smaller than the experimental result, and the underestimation is attributed to the higher order excitations which affects the shape of the well relative to prohibitively costly benchmark level calculations. While the current work provides for the first time a global PES useful for both spectroscopic and dynamic studies of this important system, it is clear that further improvements are still needed to provide a quantitatively accurate description of the system.

ACKNOWLEDGMENTS: This work was supported by the National Natural Science Foundation of China (Grant Nos. 91641104, 21590802, and 21733006), as well as the United States National Science Foundation (CHE-1566246 to R.D.) and Department of Energy (DE-SC0015997 to H. G.). Most of the calculations have been performed on the computing facilities in the High Performance Computing Center (HPCC) of Nanjing University.

View Article Online
DOI: 10.1039/C9CP02206F

References:

1. M. P. Burke, M. Chaos, Y. G. Ju, F. L. Dryer and S. J. Klippenstein, *Int. J. Chem. Kinet.*, 2012, **44**, 444.
2. A. J. C. Varandas, *Int. Rev. Phys. Chem.*, 2000, **19**, 199.
3. C. Murray, E. L. Derro, T. D. Sechler and M. I. Lester, *Acc. Chem. Res.*, 2009, **42**, 419.
4. F. Cacace, G. de Petris and A. Troiani, *Science*, 2002, **295**, 480.
5. K. Suma, Y. Sumiyoshi and Y. Endo, *Science*, 2005, **308**, 1885.
6. C. Murray, E. L. Derro, T. D. Sechler and M. I. Lester, *J. Phys. Chem. A*, 2007, **111**, 4727.
7. E. L. Derro, C. Murray, T. D. Sechler and M. I. Lester, *J. Phys. Chem. A*, 2007, **111**, 11592.
8. E. L. Derro, T. D. Sechler, C. Murray and M. I. Lester, *J. Phys. Chem. A*, 2008, **112**, 9269.
9. E. L. Derro, T. D. Sechler, C. Murray and M. I. Lester, *J. Chem. Phys.*, 2008, **128**, 244313.
10. J. M. Beames, M. I. Lester, C. Murray, M. E. Varner and J. F. Stanton, *J. Chem. Phys.*, 2011, **134**, 044304.
11. M. C. McCarthy, V. Lattanzi, D. Kokkin, O. Martinez and J. F. Stanton, *J. Chem. Phys.*, 2012, **136**, 034303.
12. P. L. Raston, T. Liang and G. E. Douberly, *J. Chem. Phys.*, 2012, **137**, 184302.
13. T. Liang, D. B. Magers, P. L. Raston, W. D. Allen and G. E. Douberly, *J. Phys. Chem. Lett.*, 2013, **4**, 3584.
14. L. Zou, B. M. Hays and S. L. W. Weaver, *J. Phys. Chem. A*, 2016, **120**, 657.
15. L. Barreau, O. Martinez, K. N. Crabtree, C. C. Womack, J. F. Stanton and M. C. McCarthy, *J. Phys. Chem. A*, 2017, **121**, 6296.
16. S. D. Le Picard, M. Tizniti, A. Canosa, I. R. Sims and I. W. M. Smith, *Science*, 2010, **328**, 1258.
17. M. Tizniti, S. D. Le Picard, A. Canosa, I. R. Sims and I. W. M. Smith, *Phys. Chem. Chem. Phys.*, 2010, **12**, 12702.
18. A. J. C. Varandas, *Int. J. Quant. Chem.*, 2014, **114**, 1327.
19. O. Setokuchi, M. Sato and S. Matuzawa, *J. Phys. Chem. A*, 2000, **104**, 3204.
20. M. E. Varner, M. E. Harding, J. Gauss and J. F. Stanton, *Chem. Phys.*, 2008, **346**, 53.
21. P. A. Denis and F. R. Ornellas, *J. Phys. Chem. A*, 2009, **113**, 499.
22. K. Suma, Y. Sumiyoshi and Y. Endo, *J. Chem. Phys.*, 2013, **139**, 094301.
23. P. A. Denis, M. Kieninger, O. N. Ventura, R. E. Cachau and G. H. F. Diercksen, *Chem. Phys. Lett.*, 2002, **365**, 440.
24. B. J. Braams and H.-G. Yu, *Phys. Chem. Chem. Phys.*, 2008, **10**, 3150.
25. M. E. Varner, M. E. Harding, J. Vázquez, J. r. Gauss and J. F. Stanton, *J. Phys. Chem. A*, 2009, **113**, 11238.
26. J. M. Anglada, S. Olivella and A. Solé, *J. Chem. Theo. Comput.*, 2010, **6**, 2743.
27. A. J. C. Varandas, *J. Chem. Theo. Comput.*, 2012, **8**, 428.
28. Y. Zhou, H. Hu, L. Li, H. Hou and B. Wang, *Comput. Theo. Chem.*, 2013, **1026**, 24.
29. M. Dupuis, G. Fitzgerald, B. Hammond, W. A. Lester and H. F. Schaefer, *J. Chem. Phys.*, 1986, **84**, 2691.
30. A. J. C. Varandas and H. G. Yu, *Mol. Phys.*, 1997, **91**, 301.
31. H.-G. Yu and A. J. C. Varandas, *Chem. Phys. Lett.*, 2001, **334**, 173.
32. A. J. C. Varandas, *Phys. Chem. Chem. Phys.*, 2011, **13**, 9796.
33. A. Karton, S. Daon and J. M. L. Martin, *Chem. Phys. Lett.*, 2011, **510**, 165.
34. W. M. F. Fabian, J. Kalcher and R. Janoschek, *Theo. Chem. Acc.*, 2005, **114**, 182.
35. B. K. Welch, R. Dawes, D. H. Bross and B. Ruscic, *J. Phys. Chem. A*, 2019, **accepted 10.1021/acs.jpca.9b04381**.
36. T. Shiozaki, G. Knizia and H.-J. Werner, *J. Chem. Phys.*, 2011, **134**, 034113.
37. K. A. Peterson, T. B. Adler and H.-J. Werner, *J. Chem. Phys.*, 2008, **128**, 084102.

View Article Online
DOI: 10.1039/C9CP02206F

38. T. Shiozaki and H.-J. Werner, *Mol. Phys.*, 2013, **111**, 607.
39. S. R. Langhoff and E. R. Davidson, *Int. J. Quant. Chem.*, 1974, **8**, 61.
40. R. Dawes, P. Lolur, J. Ma and H. Guo, *J. Chem. Phys.*, 2011, **135**, 081102.
41. R. Dawes, P. Lolur, A. Li, B. Jiang and H. Guo, *J. Chem. Phys.*, 2013, **139**, 201103.
42. M. P. Deskevich, D. J. Nesbitt and H.-J. Werner, *J. Chem. Phys.*, 2004, **120**, 7281.
43. R. Dawes, A. W. Jasper, C. Tao, C. Richmond, C. Mukarakate, S. H. Kable and S. A. Reid, *J. Phys. Chem. Lett.*, 2010, **1**, 641.
44. Y. Zhao and D. G. Truhlar, *J. Chem. Phys.*, 2006, **125**, 194101.
45. H. J. Werner, P. J. Knowles, G. Knizia, F. R. Manby and M. Schütz, *WIREs Comput. Mol. Sci.*, 2012, **2**, 242.
46. M. J. Frisch, G. W. Trucks, H. B. Schlegel, G. E. Scuseria, M. A. Robb, J. R. Cheeseman, G. Scalmani, V. Barone, G. A. Petersson, H. Nakatsuji, X. Li, M. Caricato, A. V. Marenich, J. Bloino, B. G. Janesko, R. Gomperts, B. Mennucci, H. P. Hratchian, J. V. Ortiz, A. F. Izmaylov, J. L. Sonnenberg, Williams, F. Ding, F. Lipparini, F. Egidi, J. Goings, B. Peng, A. Petrone, T. Henderson, D. Ranasinghe, V. G. Zakrzewski, J. Gao, N. Rega, G. Zheng, W. Liang, M. Hada, M. Ehara, K. Toyota, R. Fukuda, J. Hasegawa, M. Ishida, T. Nakajima, Y. Honda, O. Kitao, H. Nakai, T. Vreven, K. Throssell, J. A. Montgomery Jr., J. E. Peralta, F. Ogliaro, M. J. Bearpark, J. J. Heyd, E. N. Brothers, K. N. Kudin, V. N. Staroverov, T. A. Keith, R. Kobayashi, J. Normand, K. Raghavachari, A. P. Rendell, J. C. Burant, S. S. Iyengar, J. Tomasi, M. Cossi, J. M. Millam, M. Klene, C. Adamo, R. Cammi, J. W. Ochterski, R. L. Martin, K. Morokuma, O. Farkas, J. B. Foresman and D. J. Fox, (Wallingford, CT, 2016).
47. B. Jiang and H. Guo, *J. Chem. Phys.*, 2013, **139**, 054112.
48. J. Li, B. Jiang and H. Guo, *J. Chem. Phys.*, 2013, **139**, 204103.
49. B. Jiang, J. Li and H. Guo, *Int. Rev. Phys. Chem.*, 2016, **35**, 479.
50. B. J. Braams and J. M. Bowman, *Int. Rev. Phys. Chem.*, 2009, **28**, 577.
51. L. M. Raff, R. Komanduri, M. Hagan and S. T. S. Bukkapatnam, *Neural Networks in Chemical Reaction Dynamics*. Oxford University Press, Oxford, 2012.
52. H. Guo, *Rev. Comput. Chem.*, 2007, **25**, 285.
53. J. C. Light and T. Carrington Jr., *Adv. Chem. Phys.*, 2000, **114**, 263.
54. J. K. Cullum and R. A. Willoughby, *Lanczos Algorithms for Large Symmetric Eigenvalue Computations*. Birkhauser, Boston, 1985.
55. R. Chen and H. Guo, *J. Chem. Phys.*, 1996, **105**, 3569.
56. R. Chen, G. Ma and H. Guo, *J. Chem. Phys.*, 2001, **114**, 4763.
57. B. Ruscic and D. H. Bross, (ATcT.anl.gov, 2018).
58. W. Jiang, N. J. DeYonker and A. K. Wilson, *J. Chem. Theo. Comput.*, 2012, **8**, 460.

Table I. Geometries and energies of *trans*-HO_3, *cis*-HO_3 and i-TS calculated from the PES with a comparison with previous theoretical[32] and experimental results.[5]

Parameter	*trans*-HO_3				*cis*-HO_3			i-TS	
	This work (PES)	MRCI+Q /VTZ[32]	MRCI+Q/ CBS (this work)	Expt.[5]	This work (PES)	MRCI+Q/ VTZ[32]	MRCI+Q/ CBS (This work)	This work (PES)	MRCI+Q /VTZ[32]
$R_{O''H}$/Å	0.971	0.968	0.977	0.972	0.975	0.971	0.980	0.971	0.974
$R_{O'O''}$/Å	1.658	1.695	1.700	1.688	1.573	1.581	1.607	1.667	1.713
$R_{OO'}$/Å	1.224	1.220	1.221	1.225	1.244	1.244	1.242	1.228	1.224
$\theta_{O'O''H}$/°	96.33	95.03	94.88	90.0	96.76	96.21	95.36	97.09	94.50
$\theta_{OO'O''}$/°	110.04	110.48	110.35	111.0	111.97	111.96	111.94	112.34	112.05
$\varphi_{OO'O''H}$/°	180	180	180	180	0	0	0	81.40	77.64
ΔE/cm^{-1}	0	0	0	0	32.98	62.95	26.93	365.22	-

Table II. Comparison of calculated harmonic frequencies (in cm^{-1}) of the stationary pointes for HO_3 and DO_3 with other *ab initio* results for HO_3.[32]

trans			*cis*			i-TS		
MRCI+Q/ VTZ[32] HO_3	PES (this work) HO_3	PES (this work) DO_3	MRCI+Q /VTZ[32] HO_3	PES (this work) HO_3	PES (this work) DO_3	MRCI+Q/ VTZ[32] HO_3	PES (this work) HO_3	PES (this work) DO_3
147.6	160.9	107.7	238.5	221.7	164.8	160.2i	158.2i	132.4i
222.0	300.4	295.2	282.2	314.1	311.8	167.5	254.3	247.6
501.4	507.0	500.4	595.7	612.3	576.1	503.1	541.2	530.7
1094.3	1114.4	854.4	1221.6	1244.5	980.3	1052.2	1107.5	830.1
1421.4	1429.7	1449.4	1356.0	1385.4	1279.7	1391.8	1390.3	1355.8
3761.9	3780.0	2748.5	3721.7	3717.7	2717.7	3758.1	3768.6	2716.4

View Article Online
DOI: 10.1039/C9CP02206F

Table III. Comparison of calculated fundamental frequencies (in cm^{-1}) of HO_3 and DO_3 with experimental and previous theoretical results. Zero point energies are also presented.

			HO_3					DO_3			
			Expt.[9]	UB3LYP /VTZ[34]	HCTC /AVTZ[24]	MRCI+ Q FF[22]	this work	Expt.[9]	UB3LYP /VTZ[34]	MRCI+ Q FF[22]	this work
trans	Torsion	$1\nu_6$	128.7	169	176.80	124.7	126.9	102.22	132	99.6	100.5
	Middle O-O str.	$1\nu_5$	243.7	454	354.30	251.5	262.0	245.3	452	254.6	267.2
	O-O-O bend.	$1\nu_4$	481.9	651	649.99	465.7	482.9	462.9	623	466.3	464.2
	H-O-O bend.	$1\nu_3$	997.9	1202	1136.34	1015.2	1043.3	783.9	939	794.7	811.0
	End O-O str.	$1\nu_2$	-	1341	1351.52	-	1384.5	-	-	-	1378.4
	O-H str.	$1\nu_1$	3569.3	3563	-	3570.6	3602.5	2635.06	2628	2637.3	2656.8
	ZPE		-	-	3747.0	3541.0	3582.5	-	-	-	2926.1
cis	Torsion	$1\nu_6$	149.1	-	198.73	160.7	129.4	100.7	-	-	116.1
	Middle O-O str.	$1\nu_5$	243.6	-	323.26	218.6	264.4	381	-	-	272.4
	O-O-O bend.	$1\nu_4$	486.5	-	663.81	648.5	545.4	-	-	-	533.7
	H-O-O bend.	$1\nu_3$	1008.6	-	-	1160.4	1164.3	791.0	-	-	911.8
	End O-O str.	$1\nu_2$	-	-	-	-	1308.2	-	-	-	1312.7
	O-H str.	$1\nu_1$	3565	-	-	3538.1	3558.9	2632	-	-	2624.1
	ZPE		-	-	4135.2	-	3693.8	-	-	-	3025.4

View Article Online
DOI: 10.1039/C9CP02206F

Figure 1. Definition of the HO_3 system in (a) internal coordinates and (b) diatom-diatom Jacobi coordinates.

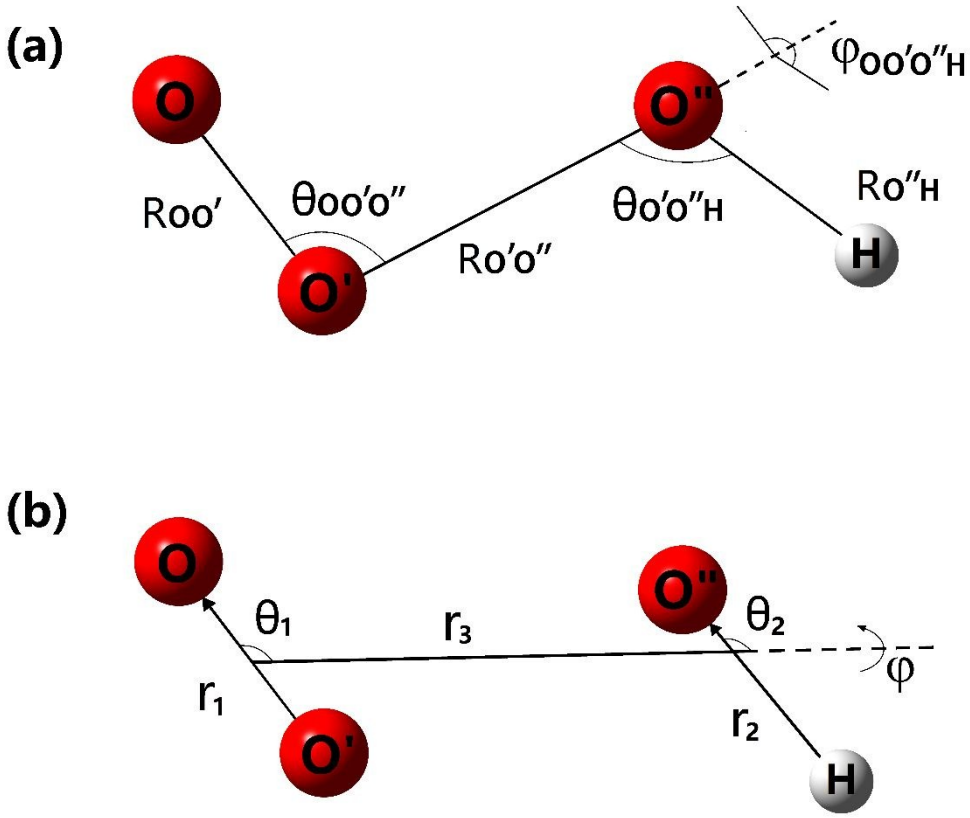

Figure 2. Plots of the three lowest $^2A''$ states computed at the MRCI+Q-F12/VTZ-F12 level along the dissociation path. The ground state switches in character with the first excited state at a distance of about 2 Å, seen as a widely avoided crossing.

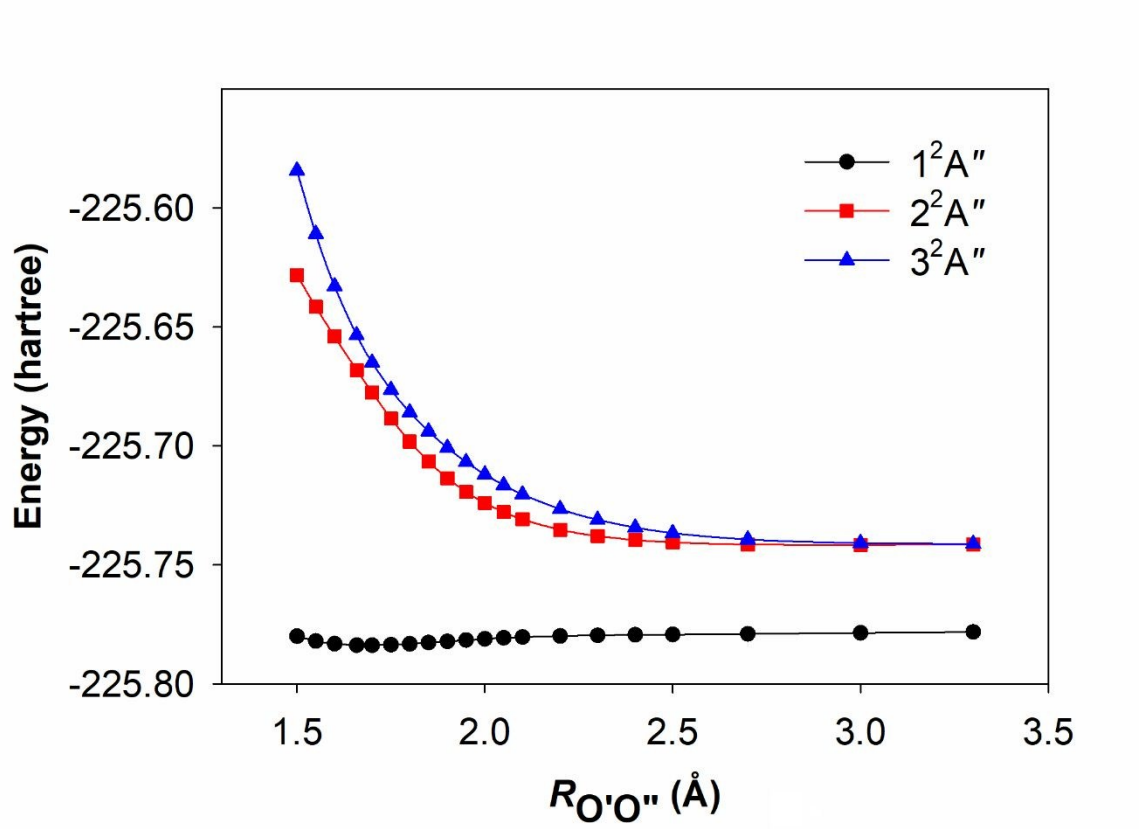

View Article Online
DOI: 10.1039/C9CP02206F

Figure 3. A plot of the nonadiabatic coupling matrix element between the two lowest states (see Fig. 2) confirms the strong interaction and switch in character that is likely the cause of spurious barriers in some reported calculations (see text).[25]

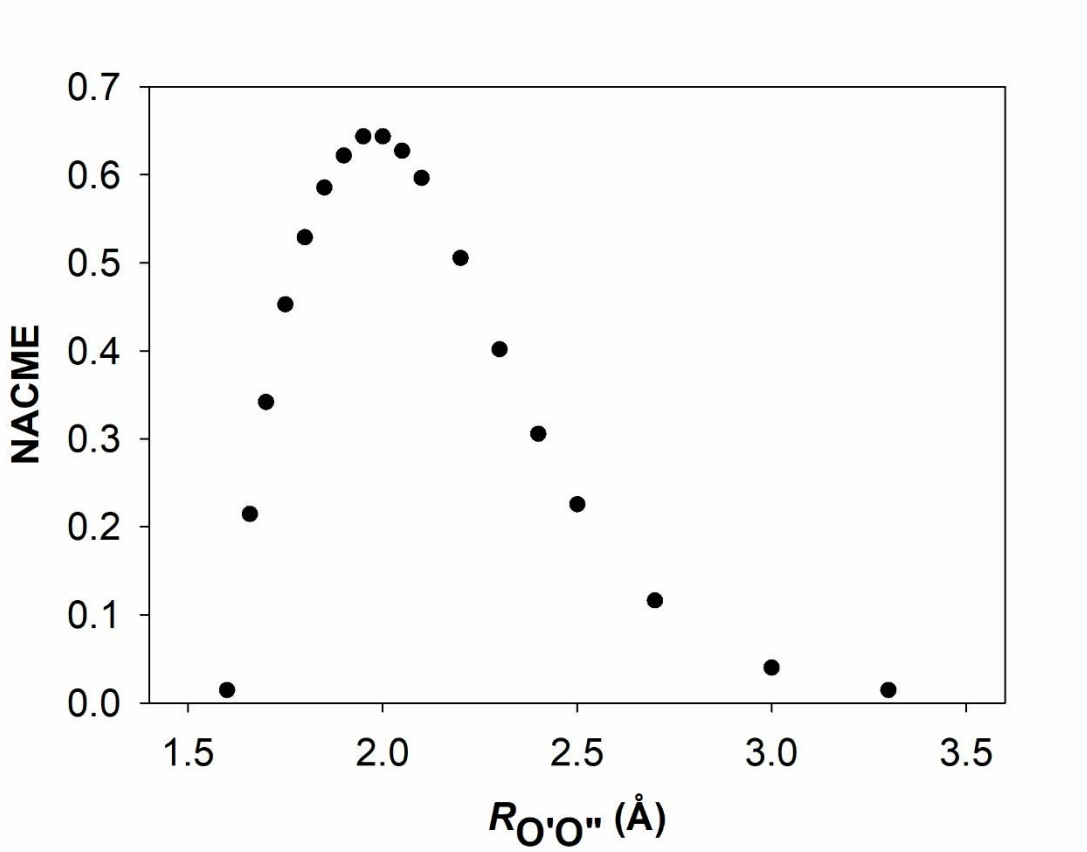

Figure 4. Distribution of fitting errors as a function of the *ab initio* energy. The energy zero is set at the *trans*-HO_3 equilibrium.

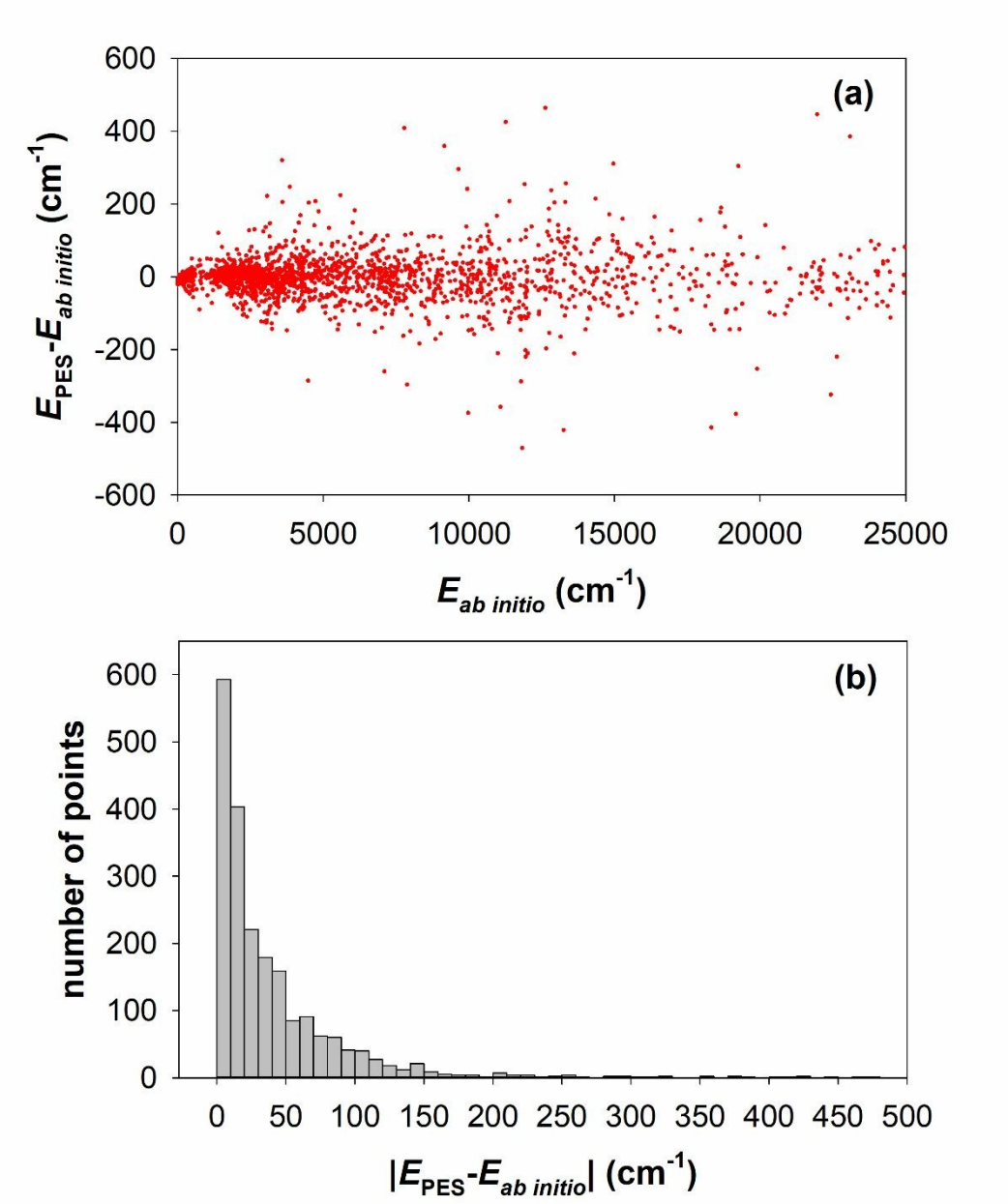

View Article Online
DOI: 10.1039/C9CP02206F

Figure 5. PES along the *cis*-HO_3 ↔ *trans*-HO_3 isomerization path, with the other four coordinates optimized. The theoretical data of Varandas[32] are also included for comparison.

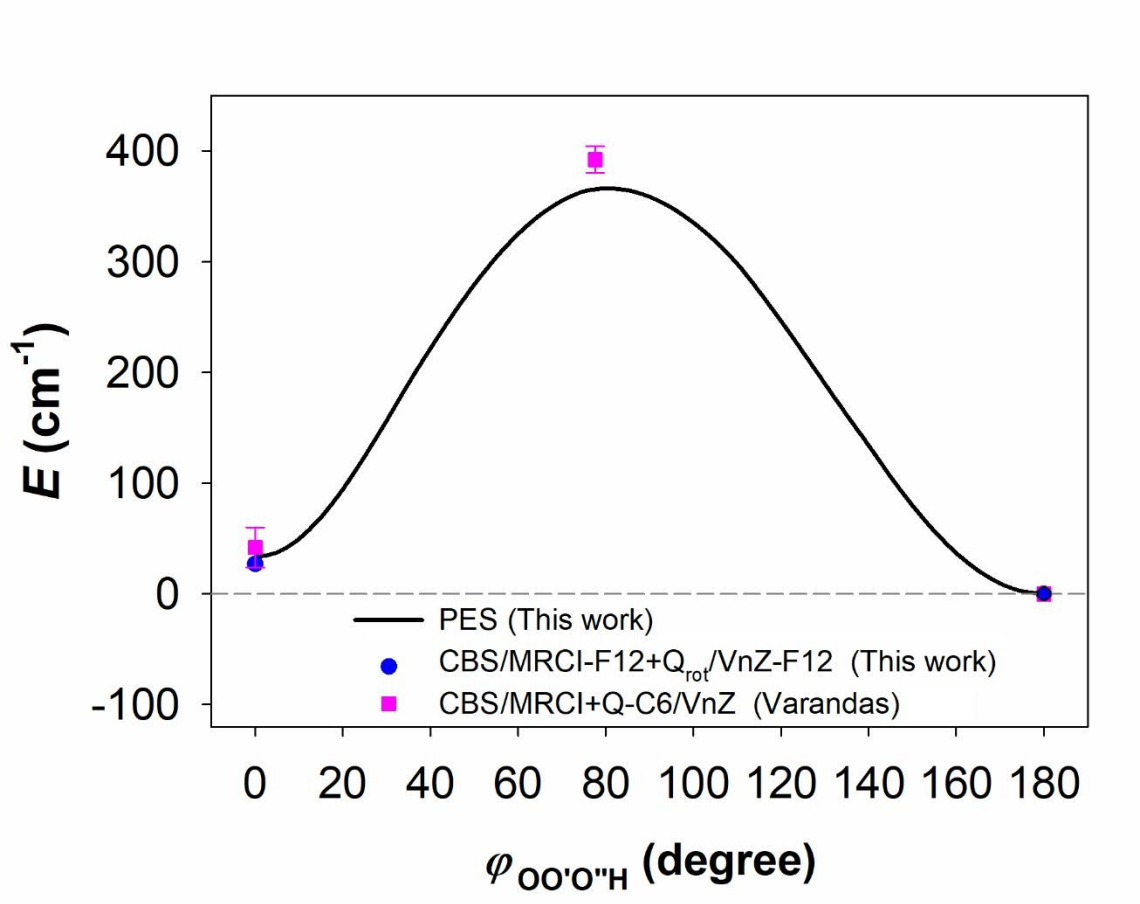

Figure 6. PES along the $HO_3 \rightarrow O_2$+OH dissociation path for both the *trans*- and *cis*-HO_3 conformers (energies taken relative to the *trans*-HO_3 minimum).

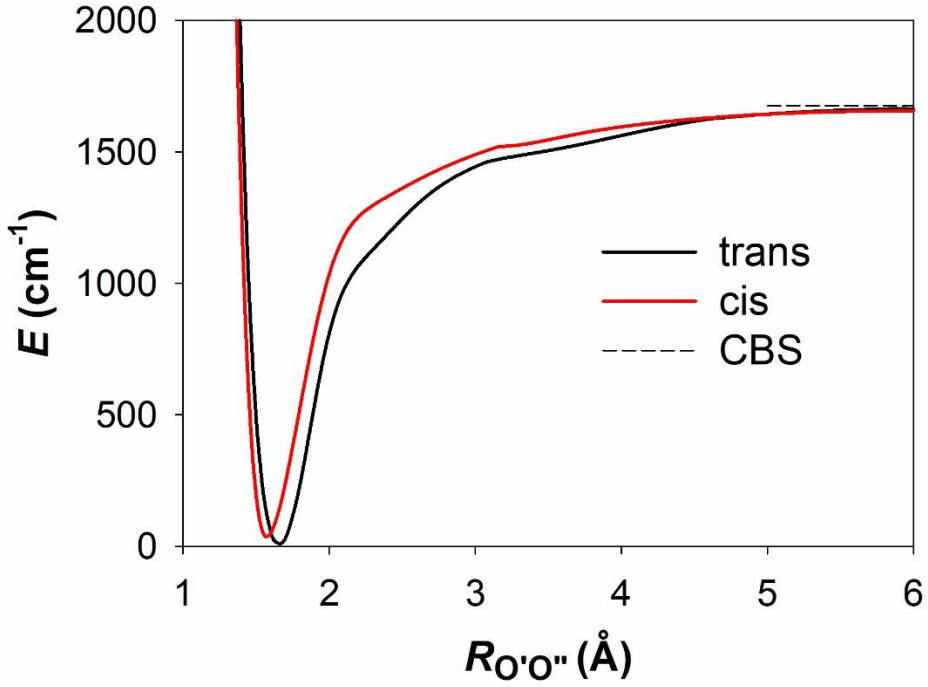

View Article Online
DOI: 10.1039/C9CP02206F

Figure 7. Contour plots of the PES in various pairs of Jacobi coordinates with other four coordinates fixed at the *trans*-HO_3 equilibrium values. The energy of the contours is given in cm^{-1}.

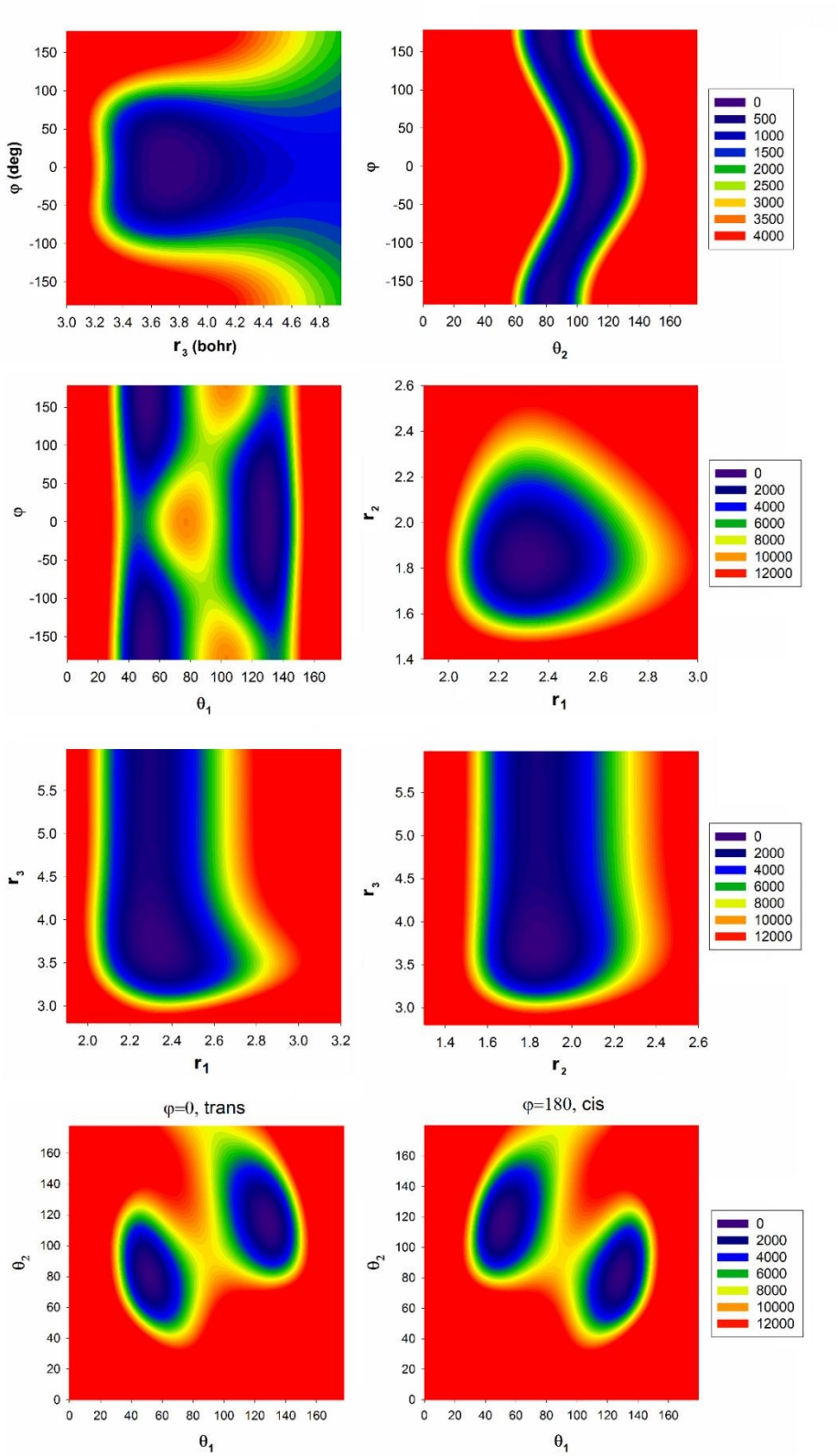

Figure 8. Cuts of wavefunctions for several low-lying vibrational states for *trans*- and *cis*-HO_3, labeled as $(n_1n_2n_3n_4n_5n_6)$ where n_i are the quantum number for the ith normal mode. The wavenumbers relative to the corresponding *trans*- or *cis*-ZPE are also indicated. The cuts are selected to maximize the wavefunction amplitudes.

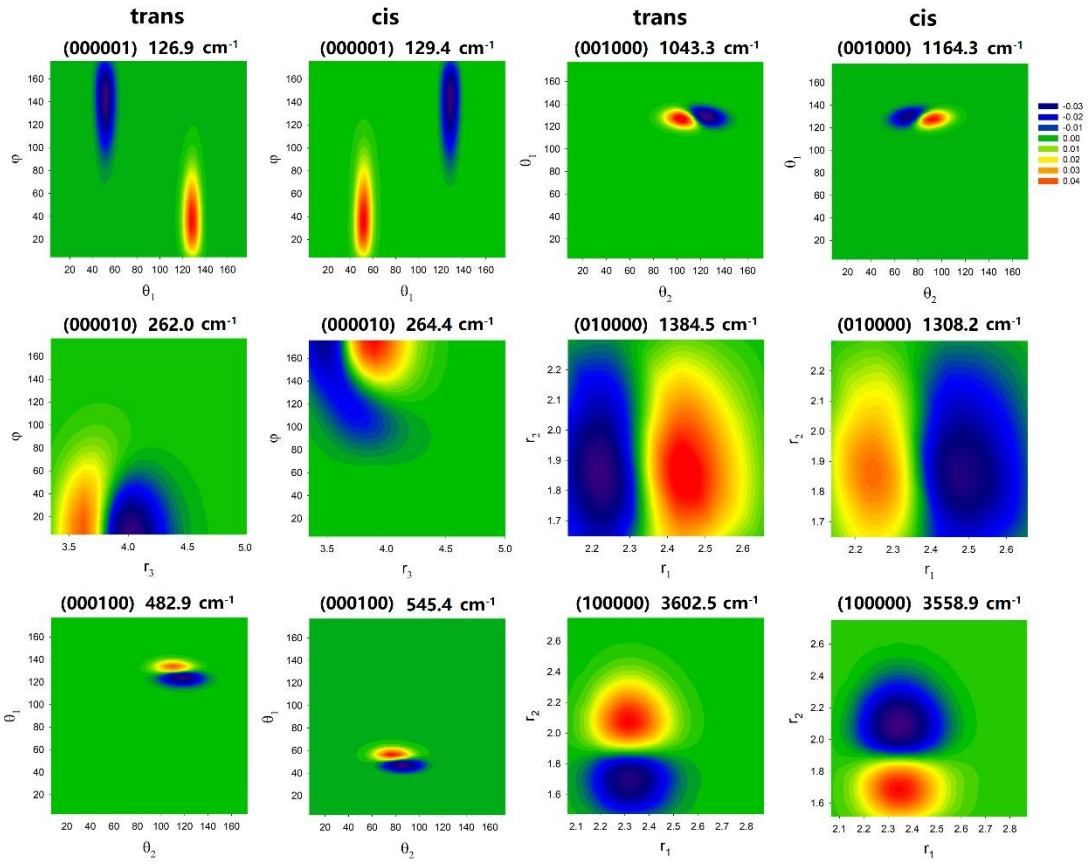

View Article Online
DOI: 10.1039/C9CP02206F

TOC graphic